Consistently Fitting Orthopaedic Casts

Cong Rao[a], Lihao Tian[a], Dong-Ming Yan[b], Shenghui Liao[c], Oliver Deussen[d], Lin Lu[a,*]

[a]*School of Computer Science and Technology, Shandong University, Qingdao, China*
[b]*National Laboratory of Pattern Recognition (NLPR), Institute of Automation, Chinese Academy of Sciences, Beijing, China*
[c]*Central South University, Changsha, China*
[d]*SIAT Shenzhen (China), University of Konstanz (Germany)*

Abstract

Personalized orthopaedic casts largely improve the comfortability and functionality for patients compared to classical plaster casts. Current attempts on the geometric modelling of customized casts have not taken the swelling of the patients' broken extremities into account that causes a gradual deformation during the healing process. Thus, the shape of the injured body parts is not constant during wearing a cast, but may change along with a decreasing swelling. In this paper, we propose a framework for generating 3D printed personal casts that consistently fit and adapt to such deformations and allow to use a single cast throughout the whole healing process. The cast consists of two layers, an outer rigid layer, which provides enough strength and protection of the body parts and an underlying flexible layer that offers adaptability to the deformations. Both layers can be fabricated with standard 3D printers and easily be assembled around the injured body parts. We show a number of 3D printed results and demonstrate the effectiveness of our approach.

Keywords: Orthopedic casts, Consistent fitting, Personalized casts

1. Introduction

Orthopaedic casts are shells that encase portions of the human body to immobilize injured bones for rehabilitation, which are high demanded for personalized design in modern society. Traditional plaster casts expose disadvantages in both the design as well as the manufacturing stage, due to various practical problems occurring for individual patients. Recent advances of digital fabrication techniques make it possible to create patient-specific 3D-printed casts at reasonable costs. Current design processes, however, still heavily rely on experts and are usually done manually, which is too inefficient for meeting the rapidly-increasing practical requirements.

Recently it has been shown that 3D printing techniques can be efficiently used to produce personalized casts for various purposes, e.g., orthopedic cast design Kelly et al. (2015), functionality-aware mechanism retargeting Zhang et al. (2017a) as well as rapid prototyping Li and Tanaka (2018). Existing approaches take sustainability, ventilation, comfort sensitivity as their objectives, and employ structures like lattice patterns Lin et al. (2016); Li and Tanaka (2018) or Voronoi tessellations Zhang et al. (2017b) to make the cast lightweight, ventilated and with controlled stiffness.

However, current automatic geometric modeling methods for orthopedic casts design do not take the swelling process into account. In most cases, swelling occurs around the injured body parts, caused by an aggregation of body fluids, tissue growth, or an abnormal movement or repositioning of the tissue. During the healing process, the swelling decreases gradually, which causes a deformation of the body shape under

*Corresponding author
Email addresses: raocongsdu@163.com (Cong Rao), tianlihao0420@gmail.com (Lihao Tian), yandongming@gmail.com (Dong-Ming Yan), lsh@csu.edu.cn (Shenghui Liao), oliver.deussen@uni-konstanz.de (Oliver Deussen), lulin.linda@gmail.com (Lin Lu)

the cast. Thus, rigid orthopedic casts may loose their contact to the underlying body parts, and in the worst case even might lose their protection. Therefore, it is necessary to consider the deformation of injured body parts in the design of customized casts in order to keep their fitness and functionality.

In this paper, we aim to design personalized casts that offer both stiff protection and consistent fitting, to the injured body shape, along with ventilation and wearing comfort. In contrast to existing approaches Lin et al. (2016); Zhang et al. (2017b), we take shape deformation caused by swelling as an additional constraint into account. To fulfill these goals, we propose a double-layered structure for 3D printed customized orthopedic casts. We first scan the injured body part and then design the two layers of our cast separately. The outer layer is rigid, created by optimized Voronoi tessellations restricted on the surface and B-Spline curve controlled carving, to provide stiffness and protection while keeping the structure lightweight. The inner layer is flexible, close to the skin, formed by well-designed deployable structures, to offer a consistent tight fitting to the body shape along the deformations caused by swelling. Both layers can be fabricated by standard 3D printers and can be easily assembled on the injured body parts. The main contributions of our approach are as follows:

- we propose a fully automatic framework for geometric optimization on given shapes and deformations to build adaptable personalized casts;
- we include the deformation of body shapes caused by swelling during wearing an orthopedic casts into our design;
- we achieve both stiffness and flexibility of the casts via a 3D printable double-layer geometric structure.

2. Related Work

Personalized casts. For years, orthopedic casts were custom-built by off-the-shelf, fixed-sized, ready-made splints, usually with Velcro straps to adjust the size for individual patients. Such splints are bulky and may cause itchy and smelly feelings for the patients. Using 3D scanning and printing techniques, designers have made highly personalized orthopedic casts. A 3D scan of the injured body parts is obtained and then the casts is designed with distributed cancellous holes, for protecting the injured area and producing comfort for wearing. The casts are ventilated, lightweight, hygienic, and to a certain degree also aesthetic Evill and Evill (2013); Karasahin (2014). However, the modeling process involves heavy manual editing of the 3D models, which requires highly experienced designers.

Kim and Jeong (2015) propose a hybrid model that separates the plastic cast into two parts, the 3D printed inner frame and an outer cover manufactured by injection molding. The combination of 3D printing and molding helps to lower the fabrication cost, although the ventilation is not considered here. To optimize ventilation and strength-to-weight properties of the casts, honeycomb patterns are carved out of the surface Zhang et al. (2017b); Ahsan and Khoda (2018). Moreover, Zhang et al. (2017b) take the thermal comfort into consideration and integrate this factor for optimizing the geometry of the cast shapes.

Lin et al. (2016) model uniformly distributed ventilation holes on the cast surface. They obtain a tight contact with the skin by adjusting the opening gap of the cast via standard Velcro straps. Similarly, Li and Tanaka (2018) introduce a design system for modeling rigid splints and use screws and Velcro straps for fastening the splint and adjusting its fit with the skin. Both methods only achieve global and large-scale fitness, but do not provide fine accommodation on local deformations caused by inflammations and swellings. We address these problems, especially the lack of a fine grain control over the adaptation to local deformations, and propose a computational solution to automatically model consistently fitting orthopedic casts.

Computationally design of flexible structures. Researchers came up with various methods for generating flexible structures to represent or approximate target shapes, and physically realized their models via 3D printing or traditional manufacturing methods. Impressive works are found for computing planar patterns for compression garments and braces Wang and Tang (2007, 2010) with both physical and geometric objectives. A group of work deals with stretchy materials such as rubber balloons Skouras et al. (2012), soft materials

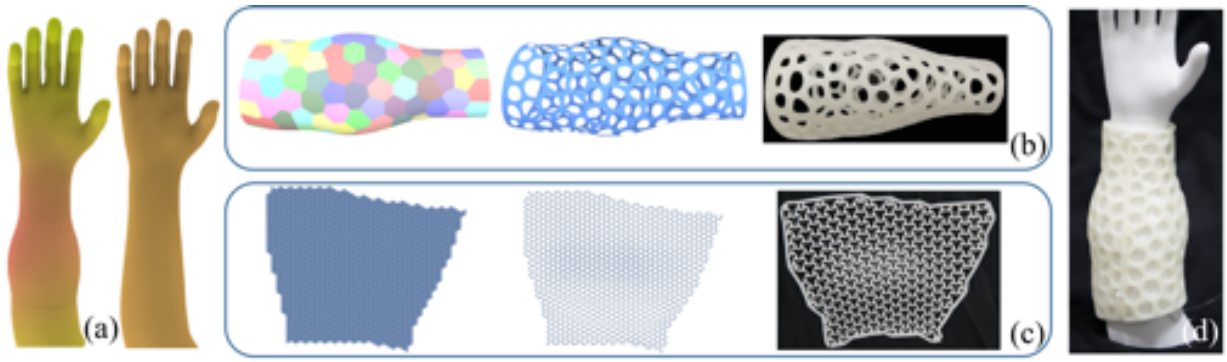

Figure 1: Given the 3D scanned models on injured and counterpart normal body parts (a), our framework generates the rigid outer cover (b) and the flexible inner layer (c) individually. The two layers are 3D printed and assembled as the orthopaedic cast that produces durable fitting on the skin (d).

with reinforced fibers Connolly et al. (2016) or embedded chambers Ma et al. (2017) to reach a desired deformation. Skouras et al. (2014) construct inflatable structures by fusing together flat sheets of nearly inextensible materials. Zhang et al. (2016b) compute a slightly stretched flattenable mesh surface that approximates the given shape with controlled strain of stretching.

Deployable structures have received much attention and been widely utilized in storage or transport thanks to the capabilities of transition between two or more geometric configurations, like Chebyshev nets Garg et al. (2014), origami patterns Dudte et al. (2016), and scissor structures. Zhang et al. (2016a) propose 2D linkages out of scissor units for designing deployable objects with two specified shapes. Zheng et al. (2016) create 3D scissor linkages that resemble user-provided 3D shapes at the most expanded state, and ensure a collision-free expansion path for sparse wireframe designs.

Konaković et al. (2016) introduce a design tool for fabricating curved target surfaces by cutting auxetic patterns into flat sheets. The method uses a uniform, fully closed initial 2D state and achieves its target state with variable partial openings. Proper deployment thus requires a guiding surface and precise manual alignment. To enable the deployment without guide surfaces, Konaković-Luković et al. (2018) directly program the target surface geometry into the flat 2D rest state. The spatially varying initial openings in 2D can be automatically deployed towards the target surface by inflation or gravitational loading. In the final deployed state, the material cannot expand any further. However, this feature is not acceptable in our setting. I.e., if the 2D linkage is of full expansion or close to it, the "underlying" tension is limited, resulting in loose contact with the target surface if the structure shrinks.

3. Overview

Besides being stiff for protection and flexible for fitting over the whole healing process, 3D printed customized casts have a number of requirements: they should be lightweight, well-ventilated, aesthetically pleasing and easy to wear. This renders the personalized cast modeling to a multi-objective optimization problem.

We propose a double-layer structure to reach these requirements. The outer layer takes the responsibility for stiffness and protection. It is created from the optimized Voronoi tessellations with smooth holes in it, while the inner layer is made from planar polyhedral patterns, is worn close to the skin, and consistently fits the skin along together with its shape changes. Both layers are fabricated individually via standard FDM-printers and assembled afterwards on the body of the patient.

As input we take a 3D-scanned model of the injured body part and its counterpart region as the normal state (most fractures happen in arms and legs, thus we always have a counterpart), see also Fig. 1a. The two layers are independent from each other in the optimization process and thus can be generated separately. The rigid/outer layer is produced by an optimized Voronoi tessellation (Fig. 1b), which is followed by

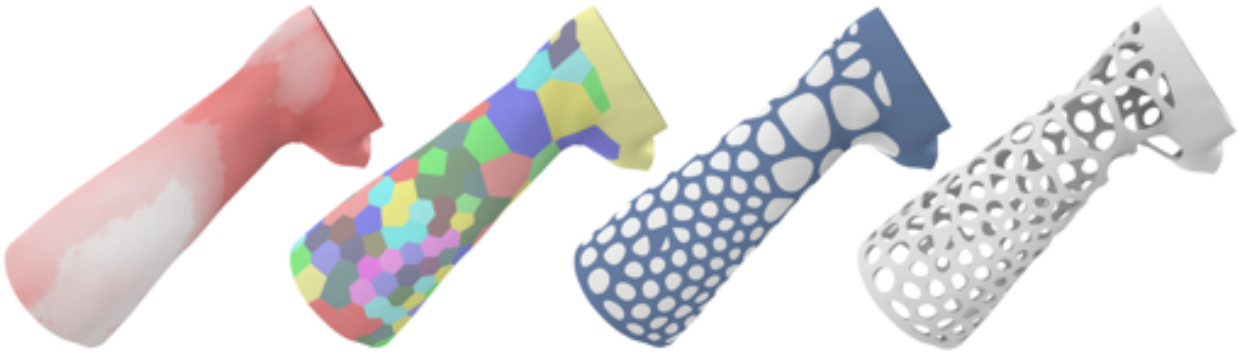

(a) (b) (c) (d)

Figure 2: Pipeline for generating the hollowed rigid cast layer: (a) temperature difference map of full cover and neutral state; (b) the corresponding centroidal Voronoi tessellation; (c) hollowed cast surface by B-Spline curve in each Voronoi cell; (d) the fabricable, solid cast with uniform thickness.

a hollowing procedure formulated by B-Spline curves. Similar to Zhang et al. (2017b), the optimization takes strength, ventilation and lightweight as objectives by considering the thermal dissipation. Specifically, we map the thermal-comfort sensitivity to an underlying density map and compute a Centroidal Voronoi Tessellation (CVT) Liu et al. (2009) on the scanned surface. After constructing a non-uniform distribution of the Voronoi cells, we compute the porous structure by creating holes along B-Spline curves in the cells. To further enhance the strength of the rigid cast in order to resist external forces, we perform a structural analysis and optimization on the thickness to obtain a smooth, stable and comforting cast layer.

For the inner layer, we employ an auxetic linkage structure Konaković-Luković et al. (2018) to provide elasticity for a consistent fitting (Fig. 1c). The inner layer is a planar linkage of rigid triangles connected by rotational joints at their vertices that could be fabricated as a flat piece. The computation of such a structure includes three steps: First, we regard the inflated surface as the target and construct an initial planar regular meshing, 2D linkages and 3D linkages following the pipeline proposed by Konaković-Luković et al. (2018). Then we adapt a 3D linkage optimization and generate two optimized 3D linkage structures taking the inflated surface and the normal surface as the target. Lastly, we map the linkage structures to the plane and optimize the 2D linkage structures under the constraints that their elasticity is always larger than zero. In the final step, we assemble the two separate layers to a consistently fitting orthopedic cast (Fig. 1d).

4. Modeling of the rigid layer

After obtaining the 3D scanning data of the patient, the medical doctor empirically defines the region that needs to be fixed and protected. We assume that there will be no deformation or dislocation of the two end boundaries of the cast, so within the process of rehabilitation these areas can be used to keep the cast immobile. Suppose that the injured surface is S, we generate an offset mesh S_o by the thickness of the inner flexible layer. The computational modeling of the rigid layer is now performed in this displaced S_o domain. Fig. 2 shows the basic pipeline for modeling the rigid cast layer on the arm.

4.1. CVT-governed distribution

For the rigid layer design, we adopt the aforementioned porous structure based on a centroidal Voronoi tessellation for air-exposure and lightness which converts the optimization into a strength-to-weight problem Lu et al. (2014) while considering thermal comfort.

Similar to Zhang et al. (2017b), we employ the Voronoi tessellation for generating the optimized partition of the surface. In contrast to them we directly integrate the thermal constraints in the optimization of the centroidal Voronoi tessellations (CVT) Liu et al. (2009), by mapping the thermal-comfort sensitivity to the

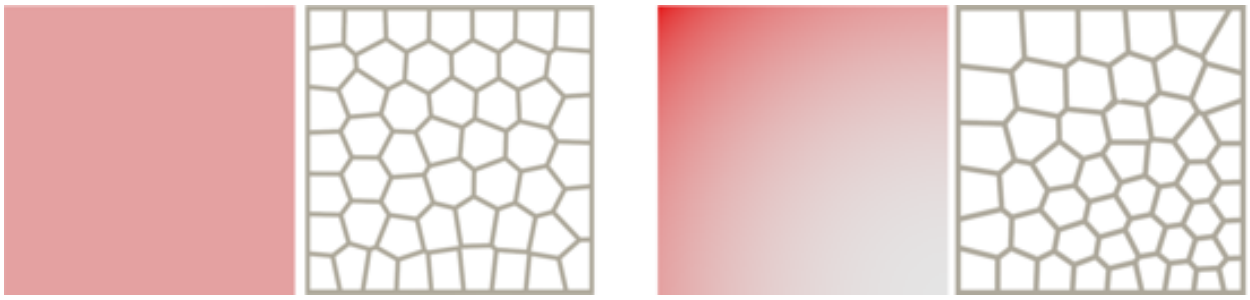

(a) (b)

Figure 3: Illustration of 2D CVTs governed by temperature sensitivity. On the left are the density map (red color indicates high thermal sensitivity and low density value) and on the right the associated Voronoi diagrams. a) uniform sensitivity; b) non-uniform sensitivity.

underlying density map. We follow the rationale in Zhang et al. (2010) as well as procedures in Zhang et al. (2017b) to obtain a temperature distribution function on nude skin when the human body feels neutrally warm and the skin fully covered, represented by $\tau(\mathbf{x})$ and $u(\mathbf{x})$ respectively, for point $\mathbf{x}$ on the surface. Then the thermal-comfort sensitivity $C(\mathbf{x})$ is formulated as:

$$C(\mathbf{x}) = \frac{12}{1 + e^{-\alpha(u(\mathbf{x})-\tau(\mathbf{x}))}} - 8. \tag{1}$$

The parameter α is 0.7 for the forearm and 0.4 for the lower leg following Zhang et al. (2017b). As $u(\mathbf{x}) \geq \tau(\mathbf{x})$, the thermal-comfort $C(\mathbf{x})$ ranges from -2 to 4. Here, a high sensitivity value indicates big variations in temperature, and thus need a large area of the cell and hollowing space. Therefore, the mapping $C(\mathbf{x})$ to the normalized underlying density function $\rho(\mathbf{x})$ on the surface is done by an inverse relationship (Eq. 2) in order to govern the CVT optimization:

$$\rho(\mathbf{x}) = (\frac{4 - C(\mathbf{x})}{6})^2. \tag{2}$$

Then, we compute the CVT restricted on the surface S_o following Yan et al. (2009), to obtain a distribution of cells following the thermal sensitivity distribution. Let $X = (\mathbf{x}_i)_{i=1}^n$ be an ordered set of n sites on S_o. The Voronoi cell for $\mathbf{x}_i$ is defined by $\psi_i = \{\mathbf{x} \in S_o | d(\mathbf{x}, \mathbf{x}_i) < d(\mathbf{x}, \mathbf{x}_j), j \neq i\}$, where $d(\cdot)$ denotes the Euclidean distance. The energy function $E(X)$ can now be written as follows

$$E(X) = \sum_{i=1}^{n} \int_{\psi_i} \rho(\mathbf{x}) d(\mathbf{x}, \mathbf{x}_i) d\mathbf{x}. \tag{3}$$

For optimization we employ the Lloyd's method Lloyd (1982) by iteratively updating the sites to the centers of the Voronoi cells to minimize the energy function. Please note that in each iteration the center of each cell is projected back on the surface S_o. Fig. 3 shows two 2D examples under uniform and non-uniform thermal sensitivity distributions. A high sensitivity drives sparse but large Voronoi cells that enable a good exposure of the skin to air when hollowing the cast.

4.2. B-Spline controlled hollowing

After constructing the CVT over the given surface, we apply a hollowing method to generate smooth cancellous holes. The basic idea follows the work of You et al. (2016), in which only 2D porous structures were discussed, though.

The hollowing process for each Voronoi cell is illustrated in Fig. 4. First, the cell ψ_i is re-scaled to form a border of r. The parameter r here implies the hollowing ratio. We set $r = 3mm$ in practice. Then, we take the new cell vertices as the control points and use them to construct a closed B-Spline curve of degree three.

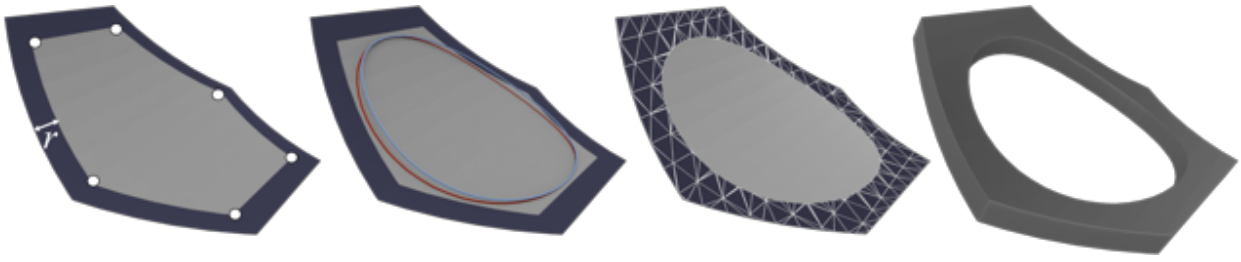

(a) (b) (c) (d)

Figure 4: Hollowing process: (a) given an arbitrary Voronoi cell, we scale it down by width r and get new vertices (white dots); (b) we take the vertices as control points and generate a close B-Spline curve (blue line), and then project it onto the original mesh (red line). (c) The hollowing mesh is constructed and extruded (d) to form a solid model.

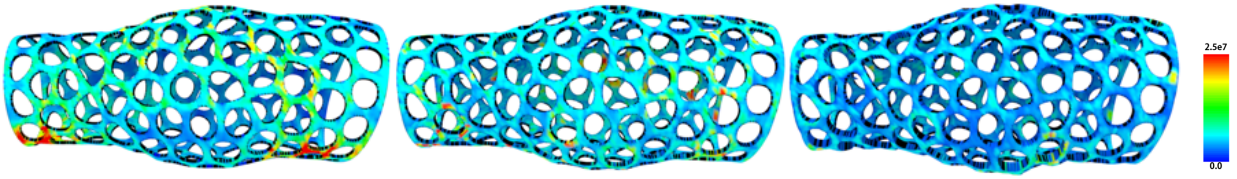

(a) (b) (c)

Figure 5: Iterations for structural optimization. Starting from the hollowed model (a) with uniform thickness (2mm), we iteratively thicken weak regions to obtain a cast which satisfies the given mechanical requirements (b-c).

We sample the closed curve and project the sampled points on the surface. Afterwards, we compute the intersection between the projected curve and the original surface S_o by splitting and remeshing triangles of the original mesh in the intersection area. Finally, we obtain a smooth, hollowed Voronoi cell. Once getting the final mesh S_h for all cells, we extrude it along the surface normal direction to get a solid fabricable model.

4.3. Structural analysis and optimization

To further enhance the stiffness of the rigid cast, we create a model with variable thickness, similar to Zhang et al. (2017b). Each vertex $\mathbf{x}$ of the hollowed mesh S_h is extruded by a thickness function, denoted by $T(\mathbf{x})$ and the solid model is represented by $Q(S_h, T(\mathbf{x}))$. The input of structural optimization is this solid model with user defined external forces and fixtures. We analyze the stress distribution by using a Finite Element Method (FEM) and obtain the von Mises stress for each element.

The goal of our optimization is to maximize the strength-to-weight ratio for the purpose of generating the lightest model with enough strength to sustain given external forces. For this we use the local thickness of the solid model as a variable of the objective function. We formulate the optimization problem by Eq. 4 where $Vol(\cdot)$ represents the volume of model, SM is the stress map computed by applying the forces F on the model Q, χ is the yielding stress value of used material (by default we use $\chi = 2.5e7N/m^2$ for PLA plastic).

$$\arg\min_{T} Vol(Q(S_h, T(\mathbf{x}))) \quad s.t. \quad SM(Q, F) < \chi \tag{4}$$

Our strategy is to locally increase the thickness of the cast to satisfy given mechanical requirements. The base model has a uniform thickness of 2mm. In each iteration, we increase the thickness of weak regions where $SM > \chi$. The iteration stops when no stress of any element is larger than χ any more, or the thickness reaches a heuristically defined upper bound of 7mm. To obtain a smooth modulation, we use a Gaussian function as a smoothing operator for local thickness editing. Fig.5 shows an example of this kind of structural enhancement.

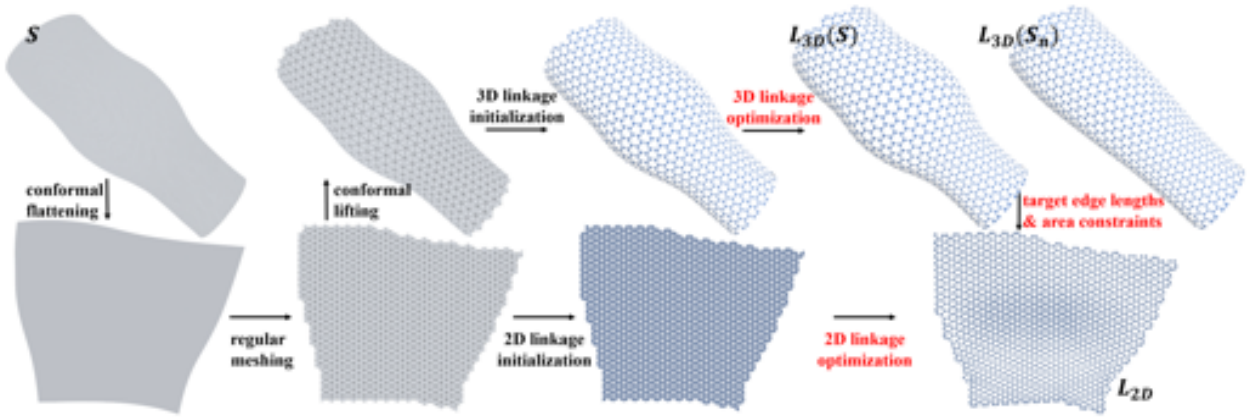

Figure 6: Computational pipeline for the flexible layer.

5. Flexible layer design

As mentioned above, we use deployable structures to form the flexible layer in order to achieve a consistent fitting with the deformable body shape. We follow the basic technique from Konaković-Luković et al. (2018) and adapt it to our problem by integrating the additional constraint that the structures need to provide a durable elasticity for the swollen as well as the normal shape of the body part. The layer is formed by polyhedral patterns that can be fabricated in a planar mode, which is very efficient and economic for standard 3D printers. When deployed, the auxetic linkages allow the material sheet to uniformly stretch and deform into the wanted curved surface. During the stretching process, the equilateral triangles of the auxetic linkage together with the hexagonal openings tile the target surface in a tri-hexagonal pattern.

The major difference to Konaković-Luković et al. (2018) is that we do not allow to reach the maximum expansion for the 2D linkages, since this implies that no elasticity in the 3D target shape would be given any more.

5.1. Computational pipeline

The objective for modelling the inner flexible layer is that it should provide consistent fitness for the injured part. In other words, the flexible layer needs to tightly cover the skin along with the deformations of the healing process, from swelling to normal states. To achieve this goal, we propose the constraint that the tension of each vertex should always be larger than zero for modelling the deployable structures.

Therefore, we 3D-scan both the injured body part S and its counterpart in the normal state S_n and use them as input shapes. The overall optimization pipeline is shown in Fig. 6. We mark the steps that are different from Konaković-Luković et al. (2018) in red and will elaborate on them in the following sections.

The optimization for generating the planar linkage structure L_{2D} has three steps: First, we regard the inflated surface S as the target and construct initial 2D and 3D linkages following Konaković-Luković et al. (2018). Second, during the 3D linkage optimization stage, we optimize the linkage structures $L_{3D}(S)$ and $L_{3D}(S_n)$ subsequently. Last, we map the linkage structure to the plane and optimize it in 2D (L_{2D}) under the constraint that the tension is larger than zero everywhere.

5.2. 3D linkage optimization

Initialization. We first compute a conformal map $f : S \to \Omega$ to transform the target surface to a planar domain $\Omega \subset \mathbf{R}^2$ using the method of Sawhney and Crane (2017). After that, we uniformly sample the domain Ω to get a planar mesh with regular equilateral triangles. The resolution for the 2D mesh is determined by the fabrication constraints. I.e., we initialize the mesh resolution to guarantee that the equilateral triangles can be realized well by 3D printing. In our experiments, edges are restricted to be larger than $8mm$ for our FDM printer. Once we have this triangle mesh, we produce an initial mesh by inversely mapping the

planar mesh onto S. The auxetic structure L_{3D} is now initialized by connecting the edge midpoints for each triangle in the initial mesh. This initial structure approximates the given surface S and will be optimized in the next step.

Optimization on $L_{3D}(S)$. To obtain the curved target configuration for the linkage, we minimize the energy function $E_{L_{3D}(S)}(\mathbf{x})$ from Eq. (5) defined as the sum of four objective terms for the vertex positions $\mathbf{x}$ with weights ω_i:

$$E_{L_{3D}(S)}(\mathbf{x}) = \omega_1 E_{expand}(\mathbf{x}) + \omega_2 E_{equi}(\mathbf{x}) + \omega_3 E_{design}(\mathbf{x}) + \omega_4 E_{boundary}(\mathbf{x}), \tag{5}$$

$$E_{boundary} = \sum_{b \in B} \|\mathbf{x}_b - P_B(\mathbf{x}_b)\|_2^2. \tag{6}$$

Here, the first three items have the same definition as in Konaković-Luković et al. (2018), i.e., E_{expand} evaluates the fully expanded mesh, E_{equi} guarantees every triangle linkage to be equilateral at different scales, E_{design} ensures that $L_{3D}(S)$ is closely approximated to S. The term $E_{boundary}$ (Eq. 6) describes the boundary constraint for the cast, i.e., the auxetic structures have fixed boundaries, aligning with the outer layer of the cast. In Eq. 6, b is a vertex index, B is the set of all vertices on the two end boundaries, and $P_B(\mathbf{x}_b)$ defines the projection of each triangle vertex to the boundary.

In the implementation, we set the weights in Eq. 5 to $\omega_1 = 2$ and $\omega_2 = \omega_3 = \omega_4 = 100$. We use a small weight for the expansion energy E_{expand} to provide space for extra expansions. A projective constraint solver based on the open-source library Deuss et al. (2015) is used for the optimization.

Optimization on $L_{3D}(S_n)$. To achieve a linkage configuration for the rehabilitated shape that is consistent with $L_{3D}(S)$, we take the linkages from $L_{3D}(S)$, project them onto the normal surface S_n and further optimize the auxetic structures by using the energy function $E_{L_{3D}(S_n)}(\mathbf{x})$ in Eq. 7, where λ_1 and λ_2 are weights for the two terms. In practice, we set $\lambda_1 = \lambda_2 = 1$. The term E_{design} now refers to the approximation of S_n and E_{edge} (Eq. 8) evaluates the variation of the edge lengths.

$$E_{L_{3D}(S_n)}(\mathbf{x}) = \lambda_1 E_{design}(\mathbf{x}) + \lambda_2 E_{edge}(\mathbf{x}) \tag{7}$$

$$E_{edge} = \sum_{(i,j) \in E} (\|(\mathbf{x}_i, \mathbf{x}_j)\|_2 - \|(\bar{\mathbf{x}}_i, \bar{\mathbf{x}}_j)\|_2)^2 \tag{8}$$

In Eq. 8, (i, j) denote the vertex indices of an edge, E is the set of edges of the linkage in $L_{3D}(S_n)$ and $(\bar{\mathbf{x}}_i, \bar{\mathbf{x}}_j)$ is the corresponding edge in the 3D linkage $L_{3D}(S)$.

5.3. 2D linkage optimization

The 3D optimization generates the nets $L_{3D}(S_n)$ and $L_{3D}(S_n)$, in which the linkages are in a partially open state. Now we need to find the contracted linkage in the plane that defines the rest state of the material to be fabricated and ensures a consistent fitting and tightness of the auxetic structure to the skin during rehabilitation till the normal state of the skin was reached.

Let H be the collection of all hexagonal openings. Each hexagonal opening $H_i \in H$ has two extreme states, the naturally flat state, and the fully expanded state. In the naturally flat state, the material is relaxed and has no extension at all, while in the fully expanded state, we regard it to have maximal extension. Based on this intuition, we employ the area to depict the tension of the hexagonal opening, and by this the elasticity of the whole structure.

Let $A(H_i)$ denote the area of H_i. $A_{flat}(H_i)$ refers to the area of H_i in flat state and $A_{max}(H_i)$ refers to the area of H_i with full expansion. Then, we have $A(H_i) < A_{max}(H_i)$ since in the 3D linkage optimization (Eq. 5) the expansion energy is controlled. The constraint that H_i is in tension, i.e., possessing tight fitting, can be described by the partial expansion state, $A(H_i) > A_{flat}(H_i)$.

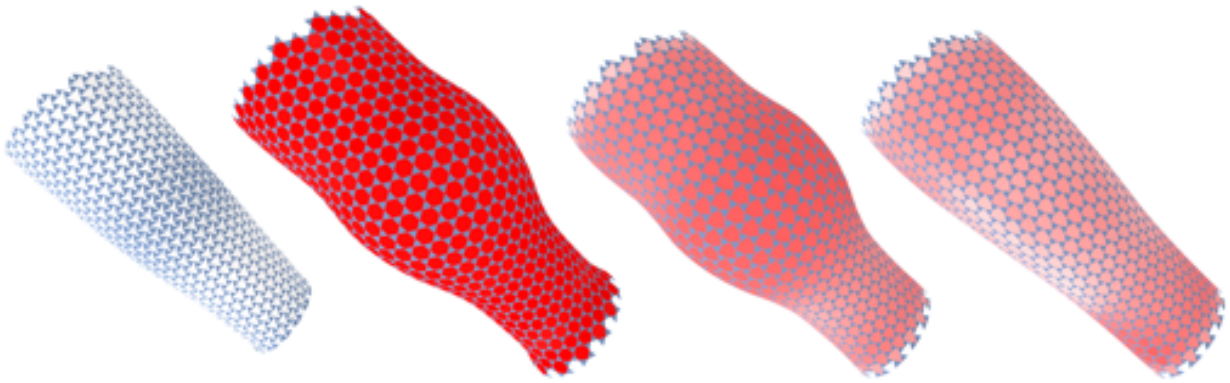

(a) (b) (c) (d)

Figure 7: The planar linkage structure L_{2D} in Fig. 6 can be rolled up in (a) without any stretch. (b) shows the maximum expansion. (c) and (d) show deformation states of the structure on the inflated and normal skin. Red color denotes a large stretch and white color indicates a small.

In Fig. 7 we color-code the value $\frac{A(H_i)-A_{flat}(H_i)}{A_{max}(H_i)-A_{flat}(H_i)}$ for each H_i, to indicate the expansion extent for each hexagonal opening, and thus the elasticity of the structure.

During flattening, our method guarantees that the edge lengths of the auxetic structure in a planar state do not change so that the auxetic structure is able to smoothly transform between the two states. Meanwhile, the area of the hexagonal openings should be less than those in the fully expanded state to provide elasticity for the consistent fitting during rehabilitating. Therefore, we formulate Eq. 9 to optimize the 2D vertex coordinates $\mathbf{u}$ of the planar auxetic structure:

$$\begin{aligned} &minimize \sum_{(i,j)\in E} (\|(\mathbf{u}_i,\mathbf{u}_j)\|_2 - \|(\mathbf{x}_i,\mathbf{x}_j)\|_2)^2 \\ &s.t. \quad \forall H_i, \quad A_{flat}(H_i) < A(H_i(S)), \quad A_{flat}(H_i) < A(H_i(S_n)). \end{aligned} \tag{9}$$

The final flat optimized auxetic surface L_{2D} is obtained by this optimization. It deploys to the desired swollen target state and maintains a tight contact with the skin till the normal state. If not, we reduce the area of the hexagonal openings in the planar state by decreasing the minimal angle of the hexagons.

Joint enhancement. As mentioned above, planar auxetic structure allows an easy fabrication by 3D printing or laser cutting. However, some constraints of fabrication accuracy and joint stability have to be considered. As an example we locally increase the material around each joint by attaching a disk to avoid fracturing while stretching, see Fig. 8b.

6. Results

We implemented our method in C++, using a Windows 10 system with an Intel® Core™ i7-7700K CPU @ 3.6GHz and 16GB RAM. We use a handhold rapid scan device of the company SHINING 3D® EinScan-Pro+ for scanning the body parts, usually done within 10 minutes. Since the thickness of the inner layer is $1mm$ in fabrication, the offset mesh S_o acting as the target surface of the outer layer is in a distance of $1mm$ to the initial surface S.

Time efficiency. Our method at the same time optimizes the outer rigid cover and the inner linkages to obtain a consistently fitting personalized cast. In the computation of outer rigid cover, we optimize the hollowed geometry and non-uniform thickness of the cast. The surface optimization has first to construct a CVT on S_o. For both CVT computation and hollowing operation, the time consumption mostly depends

on the number of sites and mesh facets. The number of sites is a user-controlled parameter, indicating the pattern distributions of the rigid cover. More sites generates denser patterns and more materials. Less sites leans to sparser distributions of Voronoi cells and less controlling freedom. Empirically, the number of sites is 100-200 based on our experiments. For optimizing the thickness, our method consumes most time for stress analysis. We use the commercial software Abaqus for stress analysis, which finishes one iteration of the optimization within 40 seconds. A model in our experiments typically needed 3-5 iterations to satisfy the given mechanical requirements.

In the optimization of the linkage structure, we need to generate the structure on the surface of the swollen and the normal parts of the human body and then flatten it for fabrication. During these procedures, time consumption mostly depends on the 2D mesh resolution and number of surface facets. Our projective constraint solver is based on the open-source library ShapeOp Deuss et al. (2015), most time is spent on projecting the auxetic structure onto the target surface.

Table. 1 summarizes the detailed timings of our algorithm. It gives information about the 3D-scanned models of different body parts, including number of facets in the mesh (*#facets*) and sites for the CVT computation(*#sites*). Furthermore, the time consumption for surface optimization (*SOpt.T.*) and thickness optimization (*TOpt.T.*) of the rigid cover is given. Timing for optimizing the flexible layer is shown in column *InOpt.T.*. The column *PlanarRes.* lists the linkage resolution, representing the number of linkages in the bounding box of the 2D mesh. Here, the number is computed by length of the edges, which is $8mm$ in our setting.

Table 1: Size of our models and duration of the optimization.

Cast	#facets	#sites	SOpt.T.(s)	TOpt.T.(s)	PlanarRes.	InOpt.T.(s)
Right Arm	28.6k	150	7	102	16*20	42
Left Arm	34.8k	150	8	170	25*32	162
Left Leg	63.8k	200	15	172	30*39	621

Table 2: Statistics of the physical casts and fabrication time.

Cast	Figure	Dimensions (mm^3)	Volume (cm^3)	OutFabT.(h)	InFabT.(h)	InCutT.(h)
Right Arm	1	145*76*81	37.98	7	3.4	1.2
Left Arm	8	188*88*82	73.91	13.5	8.3	2.6
Left Leg	10	283*134*144	161.72	25.4	14.6	3.34

Cast fabrication. The rigid outer cover is fabricated by FDM-based 3D-printing using polylactide (PLA) material and performed in two pieces that are combined to form the cast. As for the flexible inner layer, due to the fact that it is planar we can either 3D print it using thermoplastic polyurethane (TPU), or use laser cutting on polypropylene (PP) plastic sheets. Both fabrication manners can be done efficiently and at economic costs.

Table. 2 lists the size of the cast (*Dimensions*) together with the figure index (*Figure*), the final volume (*Volume*) and fabrication time of the outer rigid cover (*OutFabT.*). We also list time for fabricating the inner flexible layer in two different ways: 3D printing (*InFabT.*) and laser cutting (*InCutT.*).

Parts assembly. We stitch the inner layer using thin strings along with two corresponding side edges. Pre-designed holes (side edges) are located in non-critical parts of body part of the patients. We add a $2.5mm$ boundary of the inner layer for stitching convenience.

In order to simulate the swelling and rehabilitation of the injured body, our human models wore several sports armbands to mimic the deformations on the arm and leg shape. Fig. 9 and 11 show the deformation of our auxetic structures on the surface of left arm and left leg while the simulated habilitation process. Both elasticity distribution and real wearing results show that the flexible layer provides a consistent fitting to the skin.

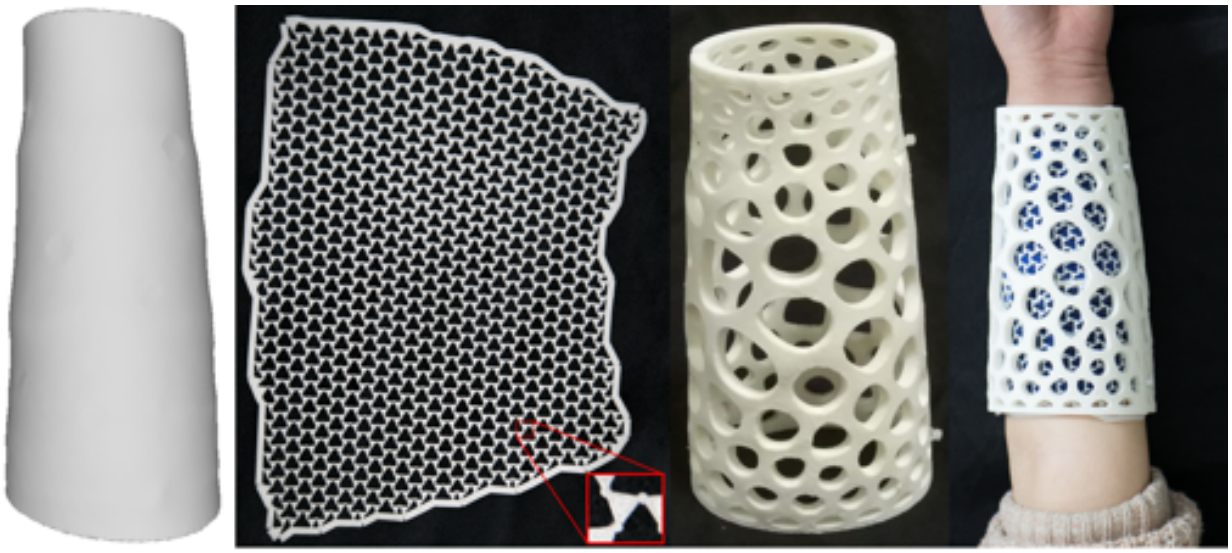

(a) (b) (c) (d)

Figure 8: Physical results of a cast for the left arm. (a) 3D-scanned swollen surface; (b) 3D-printed inner layer with TPU material; (The enlarged region shows the disk replacing each joint.) (c) 3D printed outer layer in PLA; (d) final double-layer cast on the left arm.

The two separate parts of the outer rigid cover are perforated at side edges in order to be assembled together by nylon cables. The two layers share the same end boundaries so that they are both stationary when we fix the two end boundaries of our cast. It was convenient for our test users to wear the double-layer cast. In our experiments, we spent only 3 minutes equipping the inner layer and about 20 seconds for assembling and placing the outer layer.

3D printing results and application of our casts on different parts of the human body are shown in Figs. 8 and 10. We also fabricated flexible inner layers via laser cutting, as shown in Fig. 12.

7. Conclusion and Future Work

We have proposed a novel framework for modeling personalized orthopedic casts, considering deformations of the body shapes caused by swelling and later reduction during rehabilitation. Our casts made

(a) (b) (c)

Figure 9: Flexible layer of the left arm. Top row: simulation of the deformation of the auxetic structures with the same color coding as in Fig. 7. Bottom row: physical deformation and fitting of the flexible layer worn by a user. From left to right we show the deformation during the process of rehabilitation.

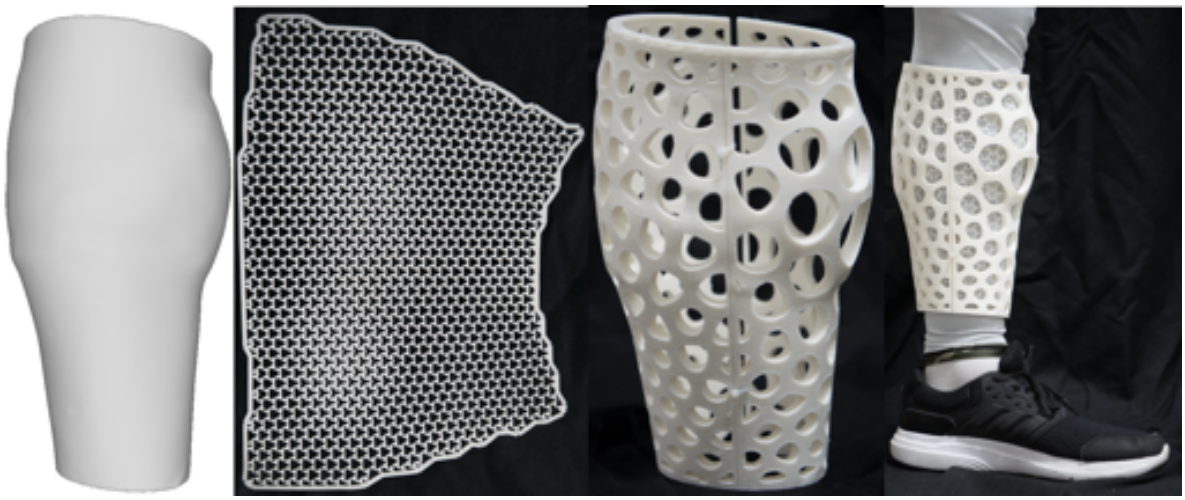

(a) (b) (c) (d)

Figure 10: Physical results of a cast of the left leg: (a) 3D-scanned swollen surface; (b) 3D-printed inner layer in TPU; (c) 3D printed outer layer in PLA; (d) the double-layer cast on the left leg.

by the combination of two layers to satisfy requirements such as stiffness, well-ventilated, lightweight, and flexible. The rigid layer is created by using optimized Voronoi tessellations restricted on the surface and smooth carved holes controlled by B-Splines. The flexible layer is formed by auxetic structures which guarantee elasticity along with shape deformations during rehabilitation. To our knowledge, this is the first attempt to provide such a fine accommodation on local deformations caused by inflammations and swellings in modelling personalized orthopedic casts. Feedback from patients that wear our casts are collected during ongoing on-site tests in hospitals. They are supposed to help us to further improve the feasibility of our proposed methods.

Limitations: One limitation of our flexible structure is that if the underlying shape is too complex, like requiring singularities, there would be many cuts in the flattening which would make the fabrication and assembly infeasible. The need to obtain the counterpart normal shape of the injured body part as an input might be hard to obtain sometimes. In such cases, we may deform the injured shape to predict the healed surface. Integrating such an automatic generation of the normal shape into our framework we see as close future work.

Acknowledgements

This work was supported by grants from National Natural Science Foundation of China (61572291, 61772523), Young Scholars Program of Shandong University (YSPSDU) and the Leading Talents of Guangdong Program (00201509).

References

Ahsan, A.N., Khoda, B., 2018. Honeycomb pattern on thin wall object with grain based 3d printing. Procedia Manufacturing 26, 900 – 911. URL: http://www.sciencedirect.com/science/article/pii/S2351978918307935, doi:https://doi.org/10.1016/j.promfg.2018.07.117. 46th SME North American Manufacturing Research Conference, NAMRC 46, Texas, USA.

Connolly, F., Walsh, C.J., Bertoldi, K., 2016. Automatic design of fiber-reinforced soft actuators for trajectory matching. Proceedings of the National Academy of Sciences URL: https://www.pnas.org/content/early/2016/12/13/1615140114, doi:10.1073/pnas.1615140114, arXiv:https://www.pnas.org/content/early/2016/12/13/1615140114.full.pdf.

Deuss, M., Deleuran, A.H., Bouaziz, S., Deng, B., Piker, D., Pauly, M., 2015. Shapeop-a robust and extensible geometric modelling paradigm.

Dudte, L.H., Vouga, E., Tachi, T., Mahadevan, L., 2016. Programming curvature using origamitessellations. Nature Materials 15, 583. URL: https://doi.org/10.1038/nmat4540.

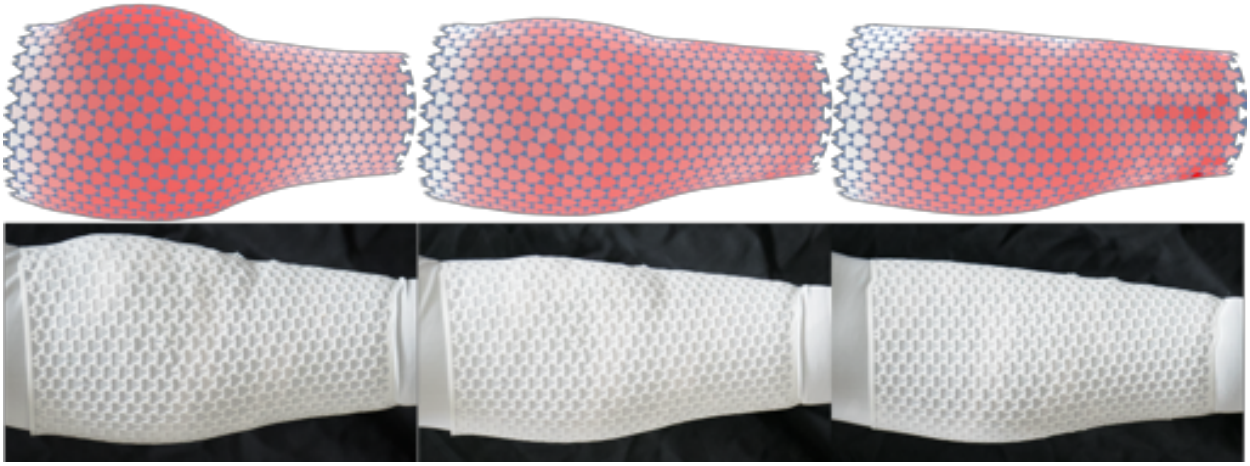

(a) (b) (c)

Figure 11: Flexible layer of a left leg. Top row: simulation of the deformation of the auxetic structures with the same color coding as in Fig. 7. Bottom row: physical deformation and fitting of the flexible layer worn by a user. From left to right we show the deformation during the process of rehabilitation.

Evill, J., Evill, O., 2013. Cortex exoskeletal cast. https://www.evilldesign.com/cortex.

Garg, A., Sageman-Furnas, A.O., Deng, B., Yue, Y., Grinspun, E., Pauly, M., Wardetzky, M., 2014. Wire mesh design. ACM Trans. Graph. 33, 66:1–66:12. URL: http://doi.acm.org/10.1145/2601097.2601106, doi:10.1145/2601097.2601106.

Karasahin, D., 2014. Osteoid medical cast. https://competition.adesignaward.com/design.php?ID=34151.

Kelly, S., Paterson, A., Bibb, R.J., 2015. A review of wrist splint designs for additive manufacture, in: Proceedings of 2015 14th Rapid Design, Prototyping and Manufacture conference (RDPM 14), Loughborough, Great Britain.

Kim, H., Jeong, S., 2015. Case study: Hybrid model for the customized wrist orthosis using 3d printing. Journal of Mechanical Science and Technology 29, 5151–5156. URL: https://doi.org/10.1007/s12206-015-1115-9, doi:10.1007/s12206-015-1115-9.

Konaković, M., Crane, K., Deng, B., Bouaziz, S., Piker, D., Pauly, M., 2016. Beyond developable: Computational design and fabrication with auxetic materials. ACM Trans. Graph. 35, 89:1–89:11. URL: http://doi.acm.org/10.1145/2897824.2925944, doi:10.1145/2897824.2925944.

Konaković-Luković, M., Panetta, J., Crane, K., Pauly, M., 2018. Rapid deployment of curved surfaces via programmable auxetics. ACM Trans. Graph. 37, 106:1–106:13. URL: http://doi.acm.org/10.1145/3197517.3201373, doi:10.1145/3197517.3201373.

Li, J., Tanaka, H., 2018. Rapid customization system for 3d-printed splint using programmable modeling technique – a practical approach. 3D Printing in Medicine 4, 5. URL: https://doi.org/10.1186/s41205-018-0027-6, doi:10.1186/s41205-018-0027-6.

Lin, H., Shi, L., Wang, D., 2016. A rapid and intelligent designing technique for patient-specific and 3d-printed orthopedic cast. 3D Printing in Medicine 2, 4. URL: https://doi.org/10.1186/s41205-016-0007-7, doi:10.1186/s41205-016-0007-7.

Liu, Y., Wang, W., Lévy, B., Sun, F., Yan, D.M., Lu, L., Yang, C., 2009. On centroidal voronoi tessellation - energy smoothness and fast computation. ACM Trans. Graph. 28, 101:1–101:17. URL: http://doi.acm.org/10.1145/1559755.1559758, doi:10.1145/1559755.1559758.

Lloyd, S.P., 1982. Least squares quantization in PCM. IEEE Transactions on Information Theory 28, 129–136.

Lu, L., Sharf, A., Zhao, H., Wei, Y., Fan, Q., Chen, X., Savoye, Y., Tu, C., Cohen-Or, D., Chen, B., 2014. Build-to-last: Strength to weight 3D printed objects. ACM Trans. Graph. 33, 97:1–97:10. URL: http://doi.acm.org/10.1145/2601097.2601168, doi:10.1145/2601097.2601168.

Ma, L.K., Zhang, Y., Liu, Y., Zhou, K., Tong, X., 2017. Computational design and fabrication of soft pneumatic objects with desired deformations. ACM Trans. Graph. 36, 239:1–239:12. URL: http://doi.acm.org/10.1145/3130800.3130850, doi:10.1145/3130800.3130850.

Sawhney, R., Crane, K., 2017. Boundary first flattening. ACM Trans. Graph. 37, 5:1–5:14. URL: http://doi.acm.org/10.1145/3132705, doi:10.1145/3132705.

Skouras, M., Thomaszewski, B., Bickel, B., Gross, M., 2012. Computational design of rubber balloons. Comput. Graph. Forum 31, 835–844. URL: http://dx.doi.org/10.1111/j.1467-8659.2012.03064.x, doi:10.1111/j.1467-8659.2012.03064.x.

Skouras, M., Thomaszewski, B., Kaufmann, P., Garg, A., Bickel, B., Grinspun, E., Gross, M., 2014. Designing inflatable structures. ACM Trans. Graph. 33, 63:1–63:10. URL: http://doi.acm.org/10.1145/2601097.2601166, doi:10.1145/2601097.2601166.

Wang, C.C., Tang, K., 2007. Woven model based geometric design of elastic medical braces. Computer-Aided Design 39, 69–79. doi:10.1016/j.cad.2006.10.001.

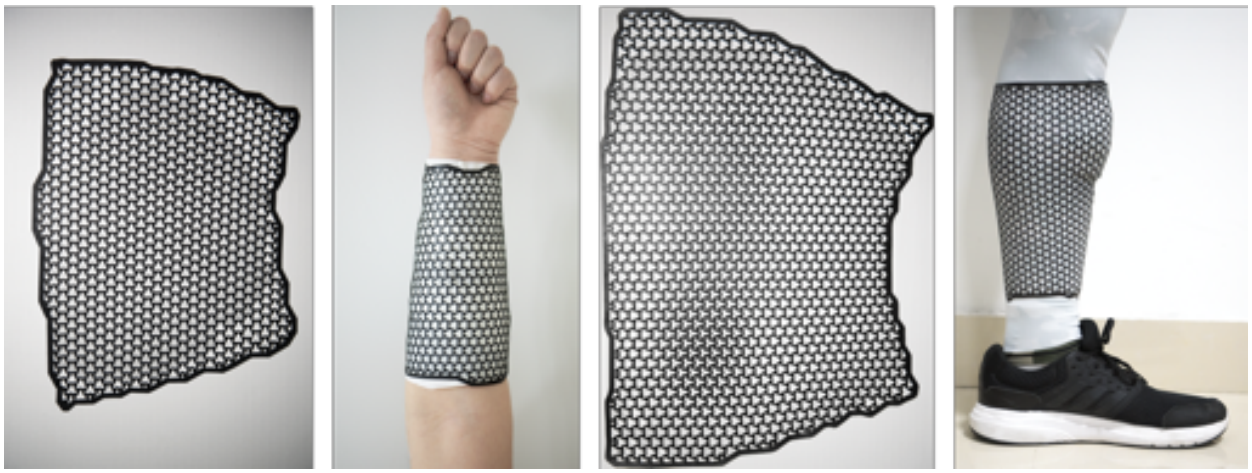

(a) (b) (c) (d)

Figure 12: Flexible layers fabricated by laser cutting: The inner layer for the left arm cut in flat state (a) and wrapped around the user's arm (b). The inner layer for the left leg in flat (c) and wrapped around the leg (d).

Wang, C.C., Tang, K., 2010. Pattern computation for compression garment by a physical/geometric approach. Computer-Aided Design 42, 78–86. doi:10.1016/j.cad.2009.02.018.

Yan, D.M., Lévy, B., Liu, Y., Sun, F., Wang, W., 2009. Isotropic remeshing with fast and exact computation of restricted voronoi diagram. Computer Graphics Forum 28, 1445–1454. doi:10.1111/j.1467-8659.2009.01521.x.

You, Y., Kou, S., Tan, S., 2016. A new approach for irregular porous structure modeling based on centroidal voronoi tessellation and b-spline. Computer-Aided Design and Applications 13, 484–489. URL: https://doi.org/10.1080/16864360.2015.1131542, doi:10.1080/16864360.2015.1131542, arXiv:https://doi.org/10.1080/16864360.2015.1131542.

Zhang, H., Arens, E., Huizenga, C., Han, T., 2010. Thermal sensation and comfort models for non-uniform and transient environments: Part i: Local sensation of individual body parts. Building and Environment 45, 380 – 388. URL: http://www.sciencedirect.com/science/article/pii/S0360132309001607, doi:https://doi.org/10.1016/j.buildenv.2009.06.018. 1st International Symposium on Sustainable Healthy Buildings.

Zhang, R., Auzinger, T., Ceylan, D., Li, W., Bickel, B., 2017a. Functionality-aware retargeting of mechanisms to 3d shapes. ACM Trans. Graph. 36, 81:1–81:13. URL: http://doi.acm.org/10.1145/3072959.3073710, doi:10.1145/3072959.3073710.

Zhang, R., Wang, S., Chen, X., Ding, C., Jiang, L., Zhou, J., Liu, L., 2016a. Designing planar deployable objects via scissor structures. IEEE Transactions on Visualization and Computer Graphics 22, 1051–1062. URL: http://dx.doi.org/10.1109/TVCG.2015.2430322, doi:10.1109/TVCG.2015.2430322.

Zhang, X., Fang, G., Dai, C., Verlinden, J., Wu, J., Whiting, E., Wang, C.C., 2017b. Thermal-comfort design of personalized casts, in: Proceedings of the 30th Annual ACM Symposium on User Interface Software and Technology, ACM, New York, NY, USA. pp. 243–254. URL: http://doi.acm.org/10.1145/3126594.3126600, doi:10.1145/3126594.3126600.

Zhang, Y., Wang, C.C.L., Ramani, K., 2016b. Optimal fitting of strain-controlled flattenable mesh surfaces. The International Journal of Advanced Manufacturing Technology 87, 2873–2887. URL: https://doi.org/10.1007/s00170-016-8669-2, doi:10.1007/s00170-016-8669-2.

Zheng, C., Sun, T., Chen, X., 2016. Deployable 3d linkages with collision avoidance, in: Proceedings of the ACM SIGGRAPH/Eurographics Symposium on Computer Animation, Eurographics Association, Goslar Germany, Germany. pp. 179–188. URL: http://dl.acm.org/citation.cfm?id=2982818.2982843.